

Atomization of correlated molecular-hydrogen chain: A fully microscopic variational Monte Carlo solution

Andrzej Biborski,^{1,*} Andrzej P. Kądziaława,^{2,†} and Józef Spałek^{2,‡}

¹Academic Centre for Materials and Nanotechnology, AGH University of Science and Technology, al. Mickiewicza 30, PL-30-059 Kraków, Poland

²Marian Smoluchowski Institute of Physics, Jagiellonian University, ulica Łojasiewicza 11, PL-30-348 Kraków, Poland



(Received 13 March 2018; revised manuscript received 24 July 2018; published 7 August 2018)

We discuss electronic properties and their evolution for the linear chain of H_2 molecules in the presence of a uniform external force f acting along the chain. The system is described by an extended Hubbard model within a *fully microscopic approach*. Explicitly, the microscopic parameters describing the intra- and intersite Coulomb interactions are determined together with the hopping integrals, by optimizing simultaneously the system ground state energy and the single-particle wave functions in the correlated state. The many-body wave function is taken in the Jastrow form and the variational Monte Carlo (VMC) method is used in combination with an *ab initio* approach to determine the energy. Both the effective Bohr radii of the renormalized single-particle wave functions and the many-body wave function parameters are determined for each f , which is the only external parameter in the whole analysis. Hence the evolution of the system can be analyzed in detail as a function of the equilibrium intermolecular distance, which in turn is determined for each f value. The transition to the atomic state, including the Peierls distortion stability, can thus be studied in a systematic manner, particularly near the threshold of the dissociation of the molecular into an atomic chain. We also show that interelectronic correlations enhance the Peierls distortion. The computational reliability of the VMC approach is also estimated.

DOI: [10.1103/PhysRevB.98.085112](https://doi.org/10.1103/PhysRevB.98.085112)

I. INTRODUCTION

Theoretical description of electronic systems, demanding a consistent incorporation of interelectronic correlations, is one of the most challenging tasks of condensed matter physics. At least two complementary strategies for finding a proper description of these complex systems are usually considered: (i) *ab initio* oriented techniques and (ii) parametrized-model approaches. The former refers primarily to the application of quantum-chemical methods, for instance the density functional theory based techniques (e.g., DFT+U, LDA+DMFT), exact diagonalization (ED), *post*-Hartree-Fock methods such as the configuration interaction (CI), Møller-Plesset perturbation theory, etc., applied to particular physical or chemical systems. The latter approaches use, e.g., the Hubbard [1] or t - J [2] models and their variants to encompass the essential features of electronic correlations such as an unconventional superconductivity observed in the cuprates [2,3], or the Mott-Hubbard [1,4] transition in transition metal oxides. Another example is the problem of the solid (molecular) hydrogen metallization at extreme pressure [5]. In fact, the last issue comprises the most of challenges, which are characteristic for both of the above mentioned methods [6–8]. It is believed that the metallization may occur by means of a transformation from the molecular crystal into the atomic one, i.e., H_2 molecules dissociation into atomic structure, which becomes metallic at a critical

pressure. This transition was first proposed by Wigner and Huntington [5] and is still under an intensive debate [9,10]. While the phase diagram of the solid hydrogen is surprisingly complex [11–13] and the predicted phase boundaries strongly depend on subtle effects such as a precise inclusion of the lattice dynamics [6,14,15], the simplified models may provide an insight into the electronic properties in the vicinity of the pressure-induced molecular-to-atomic crystal transformation. As an illustration of this, we may quote the Mott-Hubbard-like transitions proposed by us recently in the low-dimensional hydrogenic systems [16,17].

Previously, we have used the exact diagonalization + *ab initio* (EDABI) method [18–23] and could handle only a relatively small number, typically up to $N < 16$ [22–24] atoms. Therefore, we have decided to replace here the *exact* diagonalization of the Hamiltonian matrix by means of a variational Monte Carlo (VMC) solution [25–27]. This allows us to analyze the model of molecular hydrogen chain consisting of dozens of atoms and in turn to provide the quantities hardly obtainable from the exact methods, e.g., the charge gap for both the atomic and molecular phases. Moreover, the considered model can be regarded as an extension of the computational “benchmark” results for an equally spaced chain composed of hydrogen atoms [28–30], thus complementing the exact results for small-size systems. According to the Peierls theorem [31], such a chain for one electron per atom, i.e., at the *half-filling*, is unstable against spontaneous alternating distortion. However, this statement has been proved only in the absence of electron-electron correlations. The energetic stability of the electronically interacting and distorted chain were carried out both for the parametrized models (cf., e.g.,

*andrzej.biborski@agh.edu.pl

†kadzialawa@th.if.uj.edu.pl

‡jozef.spalek@uj.edu.pl

Refs. [32–34]), as well as within the paradigm of *ab initio* methods; see, e.g., Refs. [24,28,29]. The Peierls dimerization in H_n rings and (finite) chains within the full-CI formalism with the maximal $n = 14$ atoms and open boundary conditions were studied by Giner *et al.* [24]. The linear hydrogen chain and its metallic properties in the framework of the VMC method were analyzed by Stella *et al.* [28]. The state-of-art methods regarding this topic were reviewed recently by Motta *et al.* [29]. The dimerized H_2 chains but for the limited range of the lattice spacing were also investigated in the framework of the diffusion Monte Carlo method (DMC) [35].

Here we follow a different approach, in which we start from the molecular H_2 chain, the stability of which is tuned by an external force applied along the chain. We thus provide methodology analogous to our earlier EDABI-based studies [18–23]. Applying the axial force (regarded as generalized pressure) to the system—which is the sole *control* parameter—we are able to construct the phase diagram and analyze electronic properties of the chain both in the molecular (low-pressure) and nearly atomic (high-pressure) regimes. Namely, we study the chain distortion as a function of pressure and discuss the role of the system size via the finite-size-scaling procedure. In this manner, we extend the *benchmark* type of approach by following the system evolution from molecular (“Peierls-distorted”) phase to the atomiclike (metallic) phase.

In the following sections we describe the model, its parametrization, and provide computational details (cf. Sec. II). Next, we analyze the phase diagram and electronic properties of the system from the perspective of the force-induced dissociation into atomic phase. We also analyze explicitly the effect of system size as a factor of the dissociation process by performing the finite-size scaling in Sec. III. We conclude and list further related issues to be scrutinized next.

II. MODEL AND METHOD

A. Molecular chain

We consider a linear hydrogeniclike molecular chain (MLC) characterized by intermolecular distance (lattice parameter) a and bond length b (cf. Fig. 1). Note that for $b = a/2$ the system reduces to an atomic linear chain (ALC). While each molecule consists of two atomic centers assigned as α and β , the corresponding Wannier functions are $w_{i,\alpha}(\mathbf{r})$ and $w_{i,\beta}(\mathbf{r})$ for the i th molecule. Orbitals $w_{i,\mu}(\mathbf{r})$, where $\mu = \{\alpha, \beta\}$, are assumed to be *finite* contractions of $1s$ Slater atomic orbitals:

$$\psi_i^\mu(\mathbf{r}) \equiv \sqrt{\frac{\zeta^3}{\pi}} e^{-\zeta|\mathbf{r}-\mathbf{R}_i^\mu|}, \quad (1)$$

where ζ may play the role of a variational parameter and \mathbf{R}_i^μ is its atomic position. In that situation

$$w_{i,\mu}(\mathbf{r}) \approx \sum_{j(i,v)}^{L(i,\mu)} \sum_{v \in \{\alpha, \beta\}} c_{jv} \psi_j^v(\mathbf{r}), \quad (2)$$

with $L(i, v)$ and $j(i, v)$ being specific functions mapping the indices to the assumed cutoff radius $r_f = 3a$ in the tight binding approximation. Additionally, we impose the orthogonality of $\{w_{i,\mu}(\mathbf{r})\}$ basis, i.e.,

$$\langle w_{i,\mu}(\mathbf{r}) | w_{j,v}(\mathbf{r}) \rangle = \delta_{\mu\nu} \delta_{ij}, \quad (3)$$

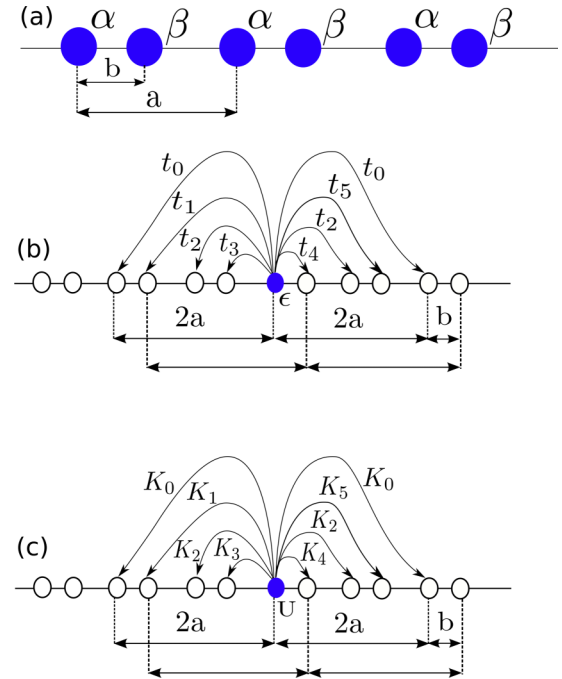


FIG. 1. (a) Schematic representation of molecular chain, characterized by lattice parameter a and bond length b ; the atomic centers of molecule are labeled as α or β . (b) Hopping terms range extends up to $2a$. Note that only one atom α (blue circle) is marked for the sake of clarity. However, by symmetry the same hopping configuration holds for β centers. (c) Same as in (b), but for the intersite (K) interactions.

which in practice is ensured in terms of performing the Löwdin symmetric orthogonalization for a block of molecules of size exceeding the interactions range (see next section). The expansion coefficients c_{jv} are taken for both atoms forming the central molecule in a block and the resulting Wannier functions $w_{i,\mu}(\mathbf{r})$ are repeated periodically. This procedure allows one to assure their mutual orthogonality within desired accuracy.

B. Hamiltonian and microscopic parameters

As in our previous works [16,17,20,22], we assume that Hamiltonian is of the extended Hubbard form, i.e.,

$$\hat{\mathcal{H}} = \sum_{i\mu} \epsilon_i^\mu \hat{n}_i + \sum_{ij\mu\nu\sigma}^i t_{ij}^{\mu\nu} \hat{c}_{i\mu\sigma}^\dagger \hat{c}_{j\nu\sigma} + U \sum_{i,\mu} \hat{n}_{i\mu\uparrow} \hat{n}_{i\mu\downarrow} + \frac{1}{2} \sum_{ij\mu\nu} K_{ij}^{\mu\nu} \hat{n}_{i\mu} \hat{n}_{j\nu} + \frac{1}{2} \sum_{ij} \frac{2}{|\mathbf{R}_i - \mathbf{R}_j|}, \quad (4)$$

where $\hat{c}_{i\mu\sigma}^\dagger$ ($\hat{c}_{i\mu\sigma}$) is the fermionic creation (annihilation) operator and the local particle number operator is $\hat{n}_{i\mu\sigma} \equiv \hat{c}_{i\mu\sigma}^\dagger \hat{c}_{i\mu\sigma}$ and counts electrons of spin σ at lattice site i and for atom labeled $\mu = \alpha, \beta$. We also define the total particle-number operator per site $\hat{n}_{i\mu} \equiv \hat{n}_{i\mu\downarrow} + \hat{n}_{i\mu\uparrow}$. The primed summations emphasize the exclusion of cases related to $i = j \wedge \mu = \nu$. One-electron matrix elements, atomic energy $\epsilon_i^\mu \equiv t_{ii}^{\mu\mu}$ and hopping amplitudes $t_{ij}^{\mu\nu}$, are defined (in the atomic units) so

that

$$t_{ij}^{\mu\nu} \equiv \langle w_{i,\mu}(\mathbf{r}) | -\nabla^2 - \sum_{l=1}^{N_S} \frac{2}{|\mathbf{R}_l - \mathbf{r}|} | w_{j,\nu}(\mathbf{r}) \rangle, \quad (5)$$

where N_S is the number of neighbors in the interaction cutoff sphere characterized by radius r_{in} . The intrasite U and intersite $K_{ij}^{\mu\nu}$ parameters are the special cases of the general form of the interaction matrix elements

$$V_{ijkl}^{\mu\nu\tau\rho} \equiv \langle w_{i,\mu}(\mathbf{r}) w_{j,\nu}(\mathbf{r}') | \frac{2}{|\mathbf{r} - \mathbf{r}'|} | w_{k,\tau}(\mathbf{r}) w_{l,\rho}(\mathbf{r}') \rangle, \quad (6)$$

i.e., $U = V_{iiii}^{\mu\mu\mu\mu} = V_{iiii}^{\nu\nu\nu\nu}$ and $K = V_{ijij}^{\mu\nu}$. We ensure that all integrals are well defined by means of assumption that $r_{in} = 2a < R_{cf}$, i.e., Eq. (2) is always fulfilled. For the sake of brevity we number all the considered hoppings $t_{ij}^{\mu\nu}$ and interaction parameters $K_{ij}^{\mu\nu}$, as in Fig. 1. According to the fact that single-electron wave functions $w_{i,\mu}(\mathbf{r})$ are real and taking into account system symmetries, selected hopping and interaction parameters are identical.

The last term in Hamiltonian (4) describes Coulomb interactions between ions which we treat in a classical manner. We neglect lattice dynamics and electron-phonon coupling, which is in principle possible to include in the VMC scheme [36,37]. In this context, its inclusion would complicate excessively our computational procedure.

C. Variational Monte Carlo

We employ the VMC method for finding an approximate ground state of the system described by Hamiltonian (4). As a variational ansatz for N -electron wave function we choose the trial state $|\Psi_T^N\rangle$ of the form

$$|\Psi_T^N\rangle \equiv \hat{\mathcal{P}} |\Phi_{FE}\rangle, \quad (7)$$

where \mathcal{P} is the Jastrow factor

$$\hat{\mathcal{P}} = \exp \left[- \sum_{i\mu, j\nu} \lambda_{i\mu, j\nu} \hat{n}_{i\mu} \hat{n}_{j\nu} - \sum_{i\mu} \lambda_{i\mu} \hat{n}_{i\mu\uparrow} \hat{n}_{i\mu\downarrow} \right], \quad (8)$$

specified by the set of variational parameters $\{\lambda_{i\mu j\nu}, \lambda_{i\mu}\}$, which provides a sufficient flexibility to include electronic correlations, while $|\Phi_{FE}\rangle$ is the solution for the system of noninteracting electrons, i.e., for the case $U = K_{ij}^{\mu\nu} = 0$. The uncorrelated solution $|\Phi_{FE}\rangle$ may be written as an expansion in the basis $\{|x\rangle\}$ spanning N -electron Fock space, i.e.,

$$|\Phi_{FE}\rangle = \sum_x c_x |x\rangle, \quad (9)$$

with

$$|x\rangle \equiv |x_\uparrow\rangle \otimes |x_\downarrow\rangle = \prod_{i\mu(|x_\uparrow\rangle)} \hat{c}_{i\mu\uparrow}^\dagger \prod_{j\nu(|x_\downarrow\rangle)} \hat{c}_{j\nu\downarrow}^\dagger |0\rangle, \quad (10)$$

where $i\mu, j\nu$ are the single-particle state indices and the total number of spin-up and spin-down electrons (n_\uparrow, n_\downarrow , respectively) are mapped from the spin-configuration sectors $|x_\uparrow\rangle$ and $|x_\downarrow\rangle$, with $|0\rangle$ being the vacuum state. The average of

an operator \hat{O} is given as

$$\langle \hat{O} \rangle \equiv \frac{\langle \Psi_T^N | \hat{O} | \Psi_T^N \rangle}{\langle \Psi_T^N | \Psi_T^N \rangle} = \frac{\sum_x \langle \Psi_T^N | x \rangle \langle x | \hat{O} | \Psi_T^N \rangle}{\sum_x \langle \Psi_T^N | x \rangle \langle x | \Psi_T^N \rangle}, \quad (11)$$

and may be expressed in terms of its local value $O_{\text{loc}}(x)$,

$$\langle \hat{O} \rangle = \sum_x \rho(x) O_{\text{loc}}(x), \quad (12)$$

where

$$O_{\text{loc}}(x) \equiv \frac{\langle x | \hat{O} | \Psi_T^N \rangle}{\langle x | \Psi_T^N \rangle} \quad (13)$$

and

$$\rho(x) \equiv \frac{\langle \Psi_T^N | x \rangle \langle x | \Psi_T^N \rangle}{\sum_{x'} \langle \Psi_T^N | x' \rangle \langle x' | \Psi_T^N \rangle} \quad (14)$$

is regarded as the probability density function. Eventually, sampling M states $|x\rangle$ from the distribution governed by $\rho(x)$ —in our case performed in a standard manner, i.e., by means of application of the Metropolis algorithm—allows one to obtain an approximate value $\langle \hat{O} \rangle$ in the form

$$\langle \hat{O} \rangle \approx \frac{1}{M} \sum_{m=1}^{m=M} O_{\text{loc}}(x_m). \quad (15)$$

In particular, the total trial energy is

$$E_T(\{\lambda_{i\mu, j\nu}, \lambda_{i\mu}\}, \zeta) = \langle \hat{\mathcal{H}} \rangle \quad (16)$$

and its variance

$$\sigma_{E_T}^2(\{\lambda_{i\mu, j\nu}, \lambda_{i\mu}\}, \zeta) \equiv \frac{1}{M} \sum_x [(\hat{\mathcal{H}} - H_{\text{loc}}(x))]^2 \quad (17)$$

can be computed. The trial energy, its variance, or a linear combination of both may be used for the optimization leading to an approximate ground state.

D. Numerical procedure

We analyze the possibility of the molecular-chain dissociation into the atomic, possibly metallic state, within a fully microscopic approach developed and tested by us earlier. The external, collinear force f is regarded here as an applied pressure on this translationally invariant 1D system. This is the sole factor, which controls such an atomization. For simplicity, we also impose the periodic boundary conditions (PBC) to eliminate the boundary effects. The proper thermodynamic potential in this case is the enthalpy [16,17] of the form

$$\frac{H}{N} = h \equiv f \frac{a}{2} + \frac{E}{N}, \quad (18)$$

where h is the enthalpy per particle and E is the system internal energy. The equilibrium value of h and the structural parameters a and b , as well as ζ at given f , are all found by means of minimization of the functional

$$h(f; a, b, \zeta) = f \frac{a}{2} + \frac{E(a, b, \zeta)}{N}. \quad (19)$$

In practice, in order to perform the optimization one must be able to compute the $E(a, b, \zeta)$ (cf. Fig. 2). The optimization run of VMC is carried out by minimizing of $\sigma_{E_T}^2$ defined

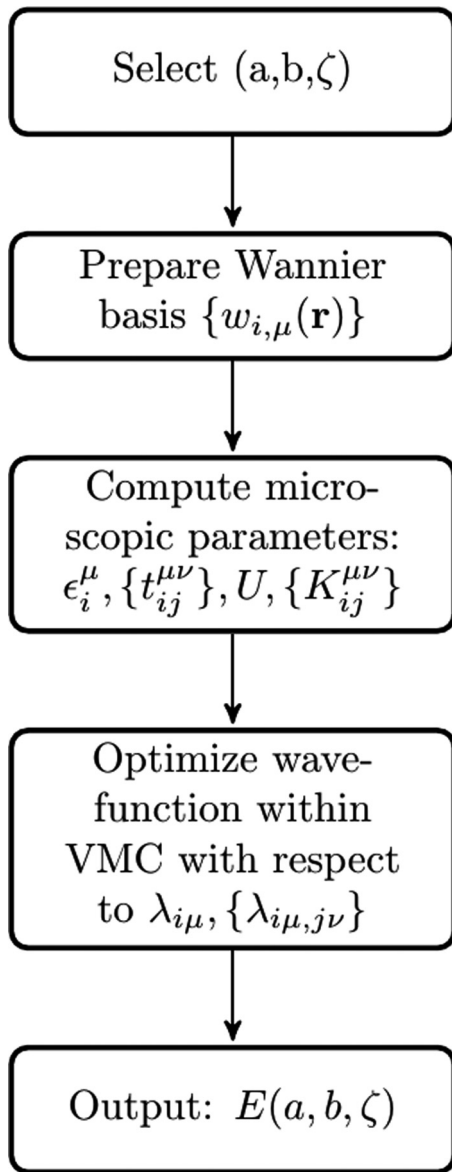


FIG. 2. Energy calculation flow chart.

by Eq. (17). This provided us with the satisfying numerical stability and is viewed as standard method in the VMC procedure [38]. Note that apart from the optimization of the Jastrow parameters, the energy must be minimized with respect to ζ . The energy which is optimized with respect to ζ in a given range of a and b allows one in turn to determine minima of $h(a, b)$. The main computational effort is optimization with respect to ζ for each considered pair (a, b) . The algorithm consists of (i) single-particle basis orthogonalization according to Eq. (3), (ii) computation of microscopic parameters according to Eqs. (5) and (6), and (iii) optimization with respect to Jastrow variational parameters and ζ . We assume the cutoff radius for Jastrow factor parameters as $r_P = r_{in} = 2a$ and, therefore, the number of interaction parameters, hoppings (with on-site atomic energy present), and the Jastrow variational parameters are equal, which amounts to seven independent quantities. The results of calculations presented in the following sections are obtained by means of self-developed codes, available

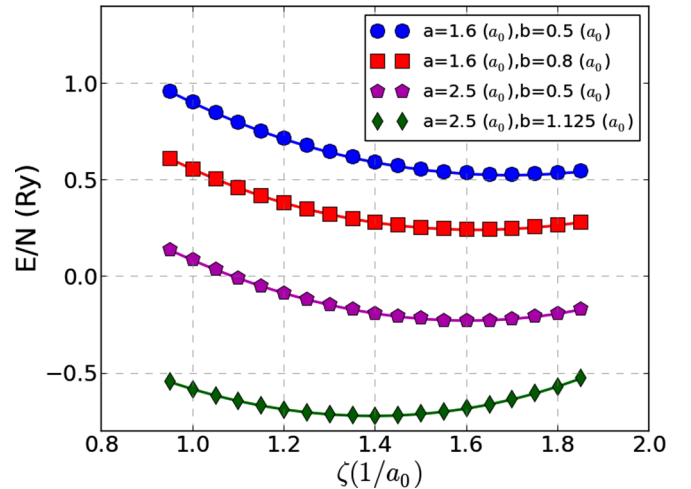


FIG. 3. Energy per electron for four different chain configurations, all as a function of variational parameter ζ for $N = 10$. The symbols refer to the data obtained by means of VMC and the solid lines are results of the exact diagonalization (EDABI). The size of the symbols is larger than the estimated statistical error, i.e., $\sim 10^{-3}$ (Ry) per electron.

from our computational library quantum metallization tools (QMT) [39].

III. RESULTS

A. Reliability of results

While the quality of results obtained by means of utilization of the selected wave-function *ansatz* [Eq. (7)] is not *a priori* known, we have performed the testing calculations for $N = 10$, i.e., the number of particles, for which our *exact* treatment is still attainable [16–23]. Precisely, we have applied the EDABI method to inspect the validity of the data obtained by means of VMC. As one may deduce from Fig. 3, where the total system energy per electron versus ζ is plotted, the agreement between the exact and VMC results is very good; typical differences do not exceed the statistical error. The energy of the system depends on ζ ; in some cases, e.g., for $a = 1.6a_0$ and $b = 0.5a_0$ (where a_0 is Bohr radius), is reduced even by factor of two when compared to the nonrenormalized case (i.e., for $\zeta = a_0^{-1}$). This observation confirms the fact that even though it increases computational complexity, the optimization with respect to ζ is important, if not indispensable. An additional remark is in place. By regarding ALC strictly as a specific variant of MLC, the number of microscopic parameters is reduced with respect to the MLC (e.g., $t_1 = t_5$). However, this implies also a similar reduction of the number of $\lambda_{i\mu j\nu}$ parameters. The number of independent $\lambda_{i\mu j\nu}$ can be increased by extending the correlation radius, but in such a scenario ALC would be solved for a different form of the many-body wave-function *ansatz*. Therefore, we have decided to introduce a small distortion $\delta b = 10^{-5}$ to the $a/2 = b$ situation, i.e., $b \rightarrow b - \delta b$. In this manner, we treat ALC as a nearly undistorted MLC to conform to the mutual consistency of the phase diagram. Results for $a/2 = b$ cases and those presented in the following subsections mean that, strictly speaking, $a/2 \approx b - \delta b$.

B. Phase diagram of finite system

We have performed detailed calculations for the systems consisting of $N = 10, 18, 26, 34, 42, 50, 66,$ and 74 electrons with the corresponding number of ions to attain the charge neutrality, and with imposed PBC. In a single VMC run, it is desired to ensure that the number of considered electrons allows for formation of a configuration closed shell [25] for the selected trial wave function. We have found out that the selection of $N = 34, 42, 50, 66,$ and 74 meets this requirement; it is not the case for $N = 10, 18,$ and 26 . Despite this shortcoming, the results obtained for $N = 10$ seem to be reasonable as might be deduced from Fig. 3, where we compare the robustness of our approach with respect to the exact treatment. However, in the finite-size-scaling analysis we utilize data obtained for five of the largest considered systems, i.e., for $N = 34, 42, 50, 66,$ and 74 . For each N we have scanned the (a, b) plane to determine the pressure (force) at which the system undergoes a transition to the atomic state. The size and range of the mesh was varied with N , since the energy landscape depends on it (see next subsection). We have assumed a constant resolution, $\Delta a = \Delta b = 0.025a_0$.

A methodological remark concerning the computational procedure is in place here. There are two factors introducing an error: the mesh resolution and the statistical error, both encoded in the bivariate interpolation. However, as the $E(a, b)$ variation is of the order of 10^{-1} Ry in the considered mesh range and the estimated statistical error is of the order of 10^{-3} Ry, the possible oscillations in the interpolation function are subtle. Namely, they are identified by us at the scale of resolution. We decided to check these interpolation affected results and, after performing the optimization procedure, we have inspected the mesh in the vicinity of (a_f, b_f) obtained at given f . This means that we identified the closest mesh nodes related to (a_f, b_f) . Next, we have been reexamining $h(a, b)$ by means of increasing/decreasing f by δf to make the enthalpy at the neighboring nodes of (a_f, b_f) the smallest possible in the mesh. In this manner, we estimated the error of f . Therefore, f_c in Fig. 9 is always related to $(a_f \pm 0.025a_0, b_f \pm 0.025a_0)$. We have been also computing $h(a_f, b_f)$ by means of the VMC procedure and the obtained results never differed by more than an order of 10^{-3} from those obtained by the interpolation. It means that the interpolation is reliable and the results obtained by VMC are consistent. Precisely, we can only say that at given f (which is the only parameter) a_f and b_f are in the ranges $a_f \pm 0.025a_0$ and $b_f \pm 0.025a_0$. Note that the mesh resolution was not taken *ad hoc*, but after many tests, which provided us with the compromise between required precision and computational time consumption.

For the sake of clarity, in this subsection we present results obtained for $N = 50$ which are representative for the whole set, whereas the important conclusions obtained from the finite-size-scaling analysis are discussed in the following subsection. Note that the results for $N = 66$ and $N = 74$ have been obtained for the subrange of (a, b) when compared to those for $N \leq 50$, due to the computational time limitations. However, we can still use these data to perform the finite-size-scaling analysis. In Fig. 4 we plot the total energy as a function of b for the selected a isolines. With the increasing $a = 1.7a_0, 1.85a_0,$ and $2.0a_0$, the two symmetric (for $b < a/2$ and $b > a/2$) minima appear and indicate the molecular chain stability (at fixed

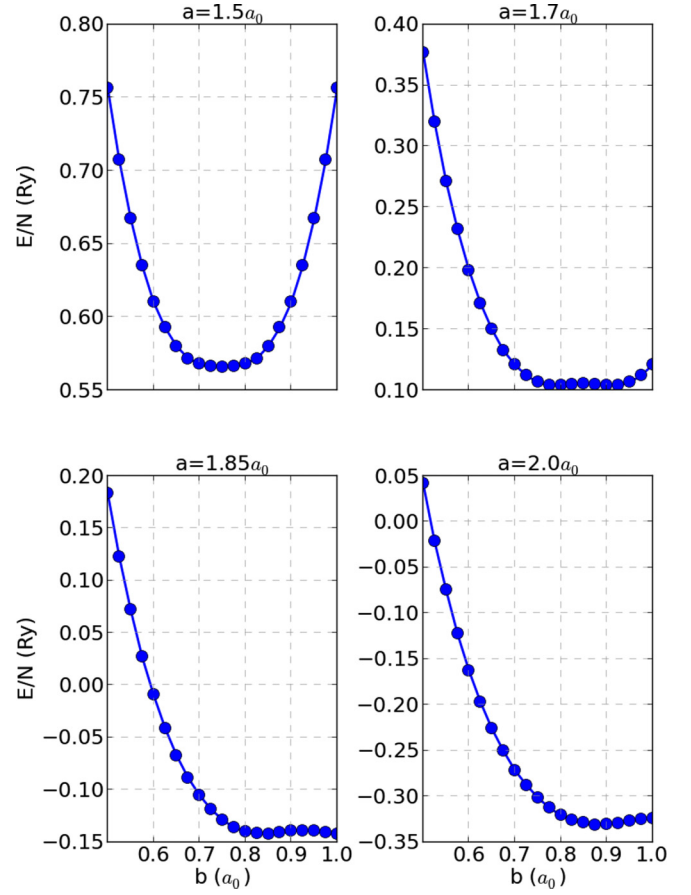


FIG. 4. Total energy as a function of b for selected $a = 1.5a_0, 1.7a_0, 1.85a_0,$ and $2.0a_0$ obtained by means of QVMC for $N = 50$. At fixed $a = 1.5a_0$ the system approaches ALC solution, i.e., the energy minimum is for $b = a/2$.

a). Results referring to $b > a/2$ are those obtained for $b < a/2$ reflected with respect to the line $b = a/2$, in accordance with the system symmetry. The evolution of the location of the minima of the enthalpy (cf. Fig. 5) are reflected in the relation between a and b (cf. Fig. 6). As the force value is below f_c , the system persists in molecular state, i.e., $a/2 > b$, whereas at f_c it becomes atomic. We observe that, while the bond length a decreases monotonically, this is not the case for b . In the vicinity of the critical force, but for $f < f_c$, the value of b increases—following the prior decrease—and finally attains the critical value $\approx a/2$. Note that the latter observation concerns maximal error. However, such a behavior is present for each considered system size. Therefore, we do not regard this as a random inaccuracy caused by the statistical noise or interpolation error.

C. Ground state energy and the critical force: Finite size scaling

As mentioned above, the results obtained for $N = 50$ represent qualitatively the trend for the other N studied. Namely, we observe atomization of the chain for each considered system size. However, we find out differences between them. In Fig. 7 we plot the energy as a function of b for $a = 1.7a_0$, for the specified values of N . The shape of the energy per atom vs b for a fixed a depends on the system size not only quantitatively, but also differs qualitatively. Namely one sees (Fig. 7) that the E

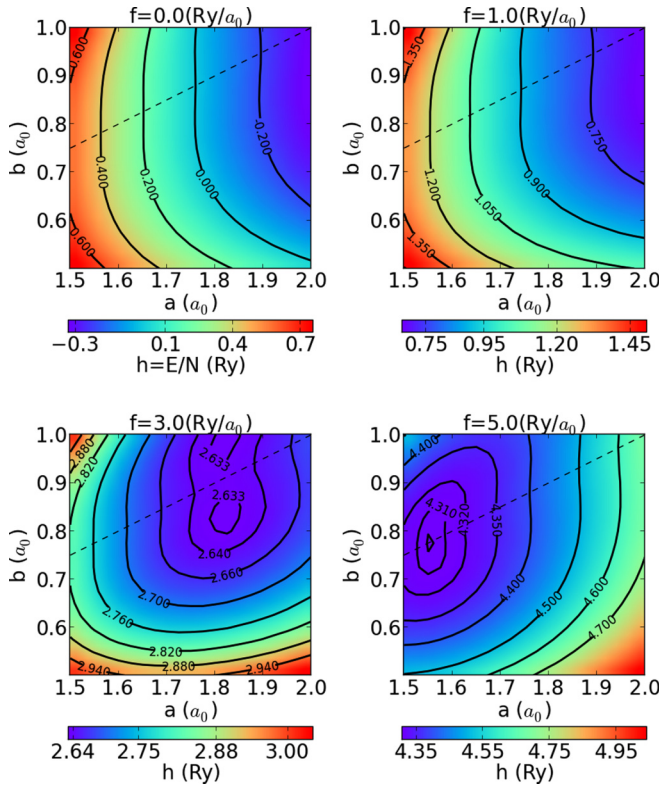


FIG. 5. Enthalpy as a function of a and b for the selected values of f and for $N = 50$. The dashed line indicates ALC. Plots are obtained from the mesh with resolution $\Delta a = \Delta b = 0.025a_0$ by smoothing it within bilinear interpolation for the sake of clarity.

minimum evolves from that corresponding to ALC for $N = 18$ as to that for $N = 26$, where it becomes flatter, suggesting a tendency towards the molecular solution. In effect, it takes place for $N \geq 42$. The energy values do not differ substantially for $b \simeq 0.7a_0$, i.e., when the system is deep in the MLC state.

We observe a *shift* of the minimum referring to the first occurrence of ALC on the $E(a, b)$ plane, i.e., to the highest possible $a/2 = b \equiv a_{\text{dim}}$ as a function of the system size (a_{dim} marks the value of a , at which the dimerization appears). This behavior was also observed for the finite chains and rings by Giner *et al.* [24]. Note that existence of $a_{\text{dim}} > 0$ in the thermodynamic limit is a *necessary* but not *sufficient* condition for the suppression of the Peierls-like state. Therefore, we checked (within the accessible accuracy), if $a_{\text{dim}}(1/N \rightarrow 0) > 0$ in the energy landscape. To answer the question if the dimerization is suppressed under for a value of force in a thermodynamic limit, we analyzed both a_{dim} and f_c as functions of $1/N$ for $N = 34, 42, 50, 66$, and 74 , in the *closed-shell* cases [25]. The $a_{\text{dim}}(1/N)$ for the considered N exhibits a linear behavior (cf. Fig. 8) so that $a_{\text{dim}}(1/N \rightarrow 0) \approx 1.77$. Therefore, to elucidate if dimerization is suppressed in the thermodynamic limit at a certain value of the applied force, we have performed finite size scaling of f_c which is shown in Fig. 9. We classify the system as ALC at $f = f_c$, which corresponds to abrupt decrease of a and concomitant abrupt increase of b , so that $a/2 \approx b$ (cf. Fig. 6). In Fig. 9 we also mark $f_c(1/N)$ with the specified polynomial function fitted to the data, obtaining $f_c(1/N \rightarrow 0) \approx 6.02 \pm 0.22(\text{Ry}/a_0)$. This value may seem to

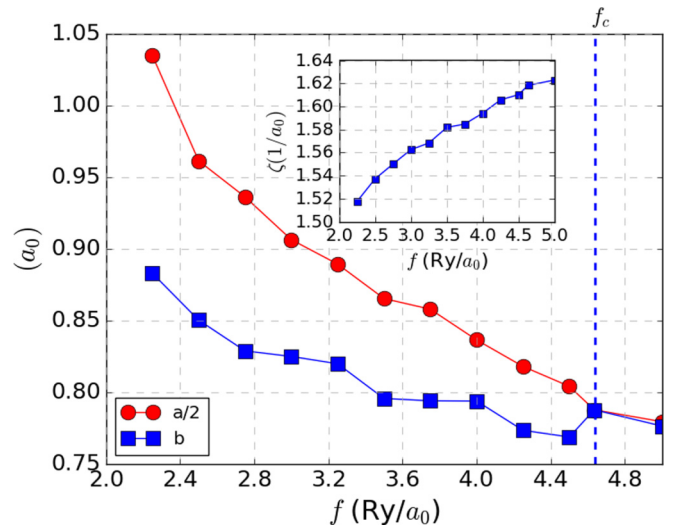


FIG. 6. Equilibrium structural parameters a and b as a function of external force f for $N = 50$. Note that we plot $a/2$ instead of a to help the identification of MLC \rightarrow ALC transition $a/2 \rightarrow b$. The critical force value is $f_c \approx 4.64 \text{ Ry}/a_0$. The inset contains corresponding dependence $\zeta(f)$. The estimated maximal error for a and b is related to the mesh resolution, i.e., $\pm 0.025a_0$.

be overestimated, since the tendency for $N = 66$ and $N = 74$ is to slightly suppress the distorted (Peierls-like) state.

For the sake of comparison we have performed also calculations of the electronically noninteracting system (cf. Sec. V). We observe that the distortion at $f = 0$ (for which this approach predicts absolute minimum of the enthalpy) is very small, i.e., $a - 2b = 1.3988a_0 - 2 \times 0.6919a_0 \approx 0.015a_0$. Therefore, it may be concluded that in the regime of the lower range of f (i.e., for $a/2 > b$), the correlations enhance the distortion magnitude.

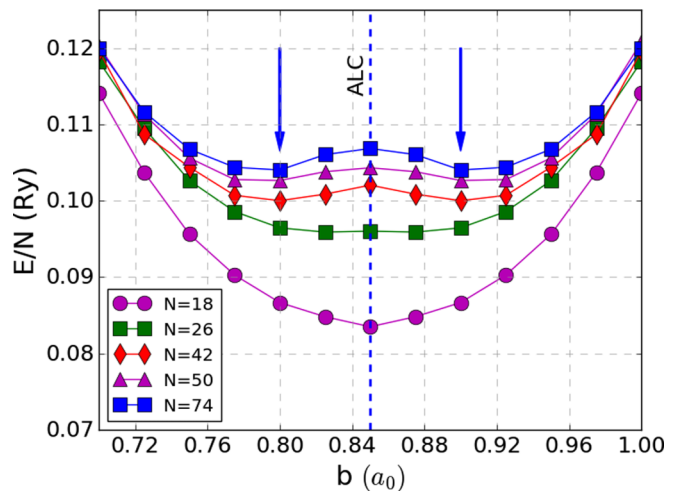


FIG. 7. Ground-state energy per electron for fixed value of $a = 1.7$ as a function of b for the selected N . Note the double minimum (marked by the arrows) appearing with the increasing system size.

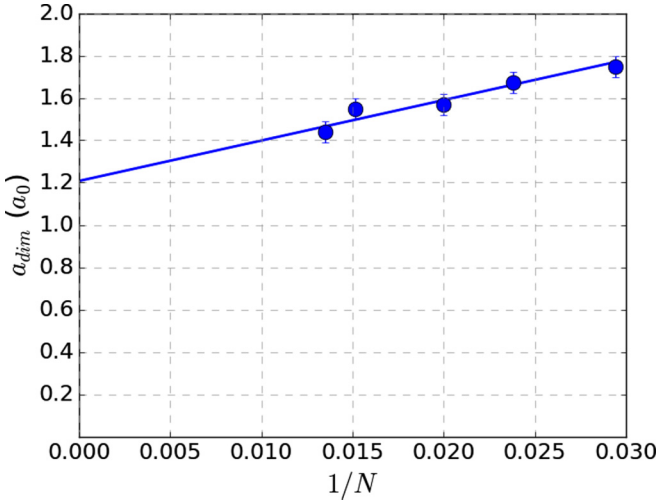


FIG. 8. Relation between a_{dim} and inverted system size N . The line indicates the linear fit.

IV. ELECTRONIC PROPERTIES

From the finite-size scaling it follows that ALC is a stable configuration for *finite* f value in the thermodynamic limit. Therefore, we provide next the basic electronic properties for both the MLC and ALC states, particularly in the regime $a/2 \approx b$.

A. Charge energy gap

To provide evidence for an insulating or metallic character of MLC close to the ALC solution we have estimated the *charge energy gap* [4,40,41]

$$\Delta \equiv [-2E(N) + E(N-4) + E(N+4)]/4. \quad (20)$$

This form of Δ allowed us to accomplish the closed-shell configuration, since for the considered system sizes (i.e., for $N \in \{34, 42, 50, 66, 74\}$) we observe the fourfold degeneracy (including spin) in $|\Phi_{FE}\rangle$ for the highest occupied and the lowest unoccupied levels. Note that N , which can be identified as the number of atomic centers, is also the number of electrons since we consider the *half-filling* case. We intended to isolate the size N as a single scaling parameter and we have not been able to perform the conclusive scaling for $a(1/N)$ and $b(1/N)$ due to the limited accuracy and maximal available value of N . Moreover, performing the scaling of $\Delta(1/N)$ for given f provides an additional complication, namely at given f the two systems of the different size, $N_1 < N_2$, may correspond to ALC and MLC solutions, respectively, which in turn reduces the available number of points to be fitted, especially close to the ALC boundary. On the other hand, we have intended to single out, at least qualitatively, the electronic characteristics of the molecular and atomic systems. Therefore, we have computed Δ for $N \in \{34, 42, 50, 66, 74\}$ for configurations $a(f)$, $b(f)$ referring to those obtained for $N = 50$. This means that microscopic parameters (hoppings, interactions, and ion repulsion) remained functions of f disregarding N . In Fig. 10 we present exemplary $\Delta(1/N)$ dependence. We have performed a set of linear fits (cf. Fig. 10) to obtain the $\Delta(1/N \rightarrow 0)$ limit by means of extrapolation,

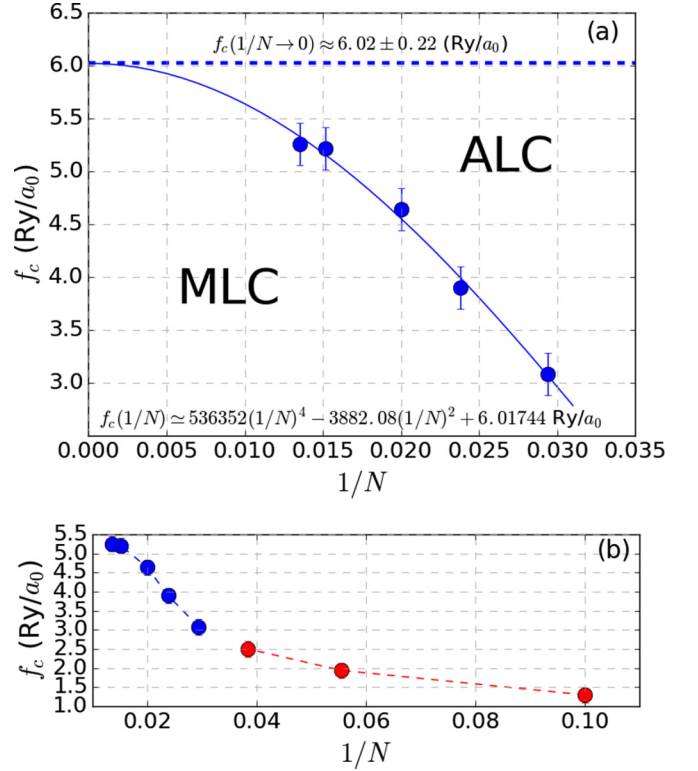


FIG. 9. (a) Critical force f_c versus the inverse system size. Points with the error bars indicate obtained values. Solid line is a polynomial fit (explicitly written at the bottom), whereas dashed line marks the estimated value of $f_c(1/N \rightarrow 0)$. The line separates the molecular (MLC) from atomic (ALC) configurations; (b) critical force for the considered chain lengths. Note that for $N < 34$ the closed-shell configuration is not fulfilled—their inclusion also prevented conclusive extrapolation and therefore they were disregarded in the final analysis. The lines are a guide for the eye.

which eventually provided $\Delta(f)$ dependence (Fig. 11). The MLC system exhibits insulating characteristics as expected for the Peierls-like state; however, in the vicinity of ALC the gap seems to be small or vanishing. In the ALC state the gap is closed, indicating the appearance of a metallic state, in agreement with the full Hamiltonian solution obtained by Stella *et al.* [28]. Indeed, for $f = 5 \text{ Ry}/a_0$, the ALC is stable with $a/2 \approx b = 0.776a_0$. This value refers to the range of $a/2$, where a hydrogenic atomic linear chain is claimed to be metallic [28]. Note also that sudden decrease of Δ to ≈ 0 at f_c coincides with that shown in Fig. 6 corresponding to molecular dissociation. The Δ quantity has also a clear dependence on the hopping ratios $-t_2/t_4$ and t_3/t_4 (cf. Appendix A for all the values of microscopic parameters), as is shown in Figs. 12(a) and 12(b). The t_2 is positive and the ratio $-t_2/t_4$ increases with increasing f . The charge gap closes at $\approx t_2/t_4 \approx 0.32$, where remains close to the value of t_2 , reaching unity in the ALC limit, as expected. The charge gap closure with the increasing $-t_2/t_4$ resembles behavior observed in the $t-t'$ Hubbard model, where the metallicity is induced by the increasing ratio between the second (t') and nearest (t) neighbor hopping amplitudes [41]. The relative (to t_4) increase of the hopping amplitude,

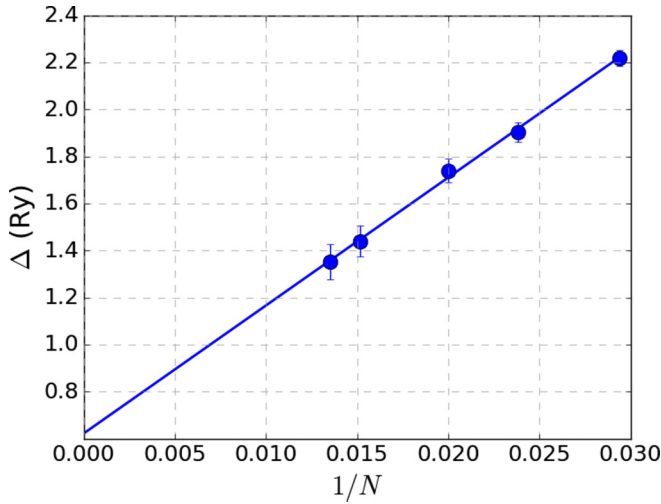


FIG. 10. Exemplary finite-size scaling of the charge gap Δ at $f = 3 \text{ Ry}/a_0$. The solid line represents the linear fit.

which we observe for t_0 , t_1 , t_2 , and t_3 , thus plays a role in the microscopic mechanism of the metallization.

B. Correlation functions

As in related studies [23,42–44] we consider next the *density-density* and *spin-spin* correlation functions to provide evidence (if any) for the charge density and spin order in the system. We define the *density-density* correlations via

$$C_{i\mu,j\nu} \equiv \langle \hat{n}_{i\mu} \hat{n}_{j\nu} \rangle - \langle \hat{n}_{i\mu} \rangle \langle \hat{n}_{j\nu} \rangle, \quad (21)$$

and the *spin-spin* correspondents

$$S_{i\mu,j\nu} \equiv \langle (\hat{n}_{i\mu\uparrow} - \hat{n}_{i\mu\sigma})(\hat{n}_{j\nu\uparrow} - \hat{n}_{j\nu\sigma}) \rangle = \langle \hat{S}_{i\mu}^z \hat{S}_{j\nu}^z \rangle. \quad (22)$$

In Fig. 13 we plot an exemplary density-density correlation function for both α and β sites. The oscillations of $C_{i\mu,j\nu}$ decay at relatively short distances. In fact, the amplitude exceeds the statistical noise only for the nearest and the next nearest

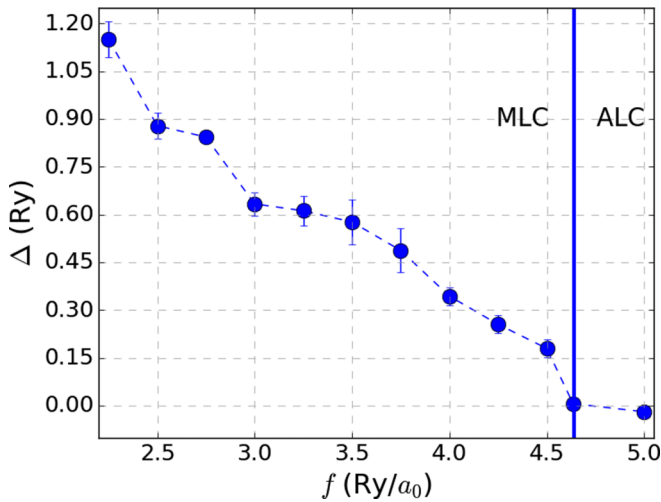


FIG. 11. Extrapolated charge gap $\Delta(f)$ for $a(f)$, $b(f)$ referring to $N = 50$ (see text). The vertical line separates MLC and ALC (for $N = 50$), whereas the dashed line is a guide for the eye.

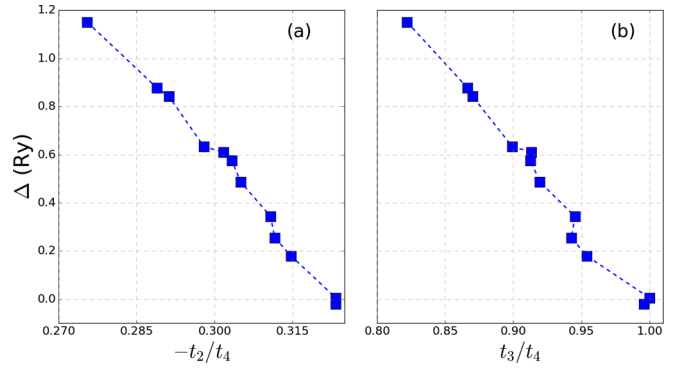


FIG. 12. Charge energy gap as a function of the selected ratios between hoppings.

neighbors which correspond to the distances $r_{j\nu} = b$ and $r_{j\nu} = a - b$, respectively. In effect, we have not found any long-range charge/spin order in both the MLC and ALC states. This may originate from the form of the trial wave function, which does not include long-range correlations.

V. SUMMARY AND CONCLUSIONS

In this work, we have analyzed the case of uniform compression of the molecular-hydrogen linear chain by means of the variational Monte Carlo method combined with the *ab initio* approach, with the help of which we have determined among others the renormalized single-particle wave function in the correlated state. Thus we have complemented the *benchmark* model of the atomic linear chain with the analysis of its stabilization under influence of the external force, starting from the linear arrangement of the molecules (MLC). We have investigated the possibility of *dissociation* of the molecular chain into the atomic linear chain within available accuracy. With the help of the finite size scaling analysis we have obtained the conditions for stabilization of the atomic phase. However, we are far from claiming that the

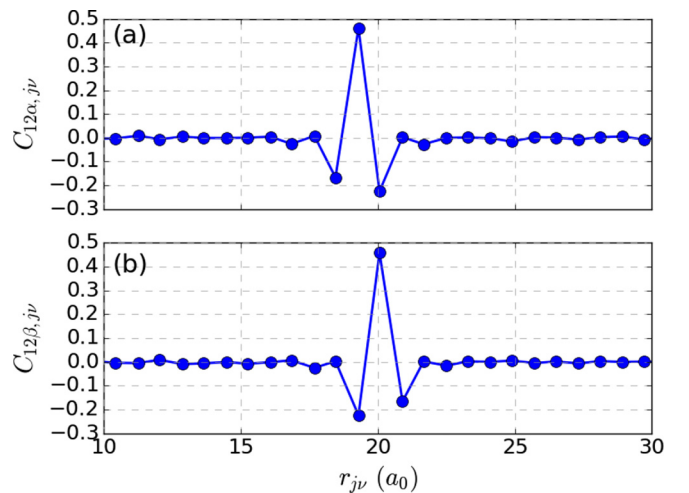


FIG. 13. Density-density correlation functions plotted for the results obtained at $f = 4.5 \text{ Ry}/a_0$ and $N = 50$ for both α (a) and β (b) sites, respectively.

distortion is completely suppressed at a finite force according to the numerical precision, applied wave-function ansatz, and the simplified form of the Hamiltonian. Despite this uncertainty, we emphasize that a particular system configuration and its electronic state is tuned solely by means of a single controllable external parameter—the force f . In that sense, by considering one-dimensional enthalpy h , we provided a thermodynamic solution for the system at $T = 0$ K. It is also sometimes postulated for the solid hydrogen phases to become metallic before occurrence of the expected atomization, i.e., it is in the molecular state by means of the band gap closure [45]. Therefore, we have analyzed the charge gap for the molecular chain in the vicinity of the arrangement close to the atomic state to find out if it exhibits metallic properties. With attainable precision, we observed a vanishing gap indicating the presence of a metallic state which coincides with the chain atomization. A qualitative analysis of the correlation functions allowed us to show the absence of a nontrivial charge and spin order.

The role of an external force f is crucial. Previously, we analyzed the ladder-type stacking of H_2 molecules [16] and have shown that such a lateral arrangement is energetically stable even for $f = 0$. This is not the case here and physically the role of the force f may be played by a substrate on which the chain is placed. In the situation in which the substrate lattice parameter is commensurate with the intermolecular distance, we can regard the force f as a uniform compressing action on the chain. A variable force could appear by changing either the substrate parameter or studying the system on different substrates.

Our analysis allows for the Peierls-distortion evolution to be characterized by the parameter

$$\delta \equiv \frac{a - 2b}{a}. \quad (23)$$

Namely, one sees that the correlations enhance the distortion in the molecular state, but it practically ceases to exist at the atomization (metallic) threshold. Our results describe a systematic study of the distortion stability. Only a very small, residual value of $\delta \neq 0$ remains in the metallic phase. The two latter results are represented in Figs. 14 and 15, respectively. Explicitly, in Fig. 14 we present schematically together the $a/2$ and b distances, the Peierls distortion δ , and the charge gap, defined by Eq. (20). Those quantities characterize the atomization (a) at $f = f_c$, the associated disappearance of appreciable Peierls distortion, originally caused by the chemical bonding into the molecular state (b), and disappearance of the charge gap at that point (c). All these characteristics, in conjunction with behavior of the density and spin correlations (cf. Fig. 13), show that the atomization takes place for a standard type of metallic state. This conclusion has been also reached in our analysis of metallization of H_2 ladders [16] that the atomic phase is close to a moderately, if not weakly, correlated and thus standard, metallic state. However, this means that the role of the electron-lattice interaction in the atomized state may also become important, as stated in a number of recent papers (see, e.g., Ref. [46]), but this subject will not be discussed here. Finally, one may ask a basic question: how does the ordinary Peierls distortion picture fit into the above picture, since the results depicted in Fig. 14(b) do not show any $\delta \neq 0$ for $f \geq f_c$? To address this question, we have plotted concrete

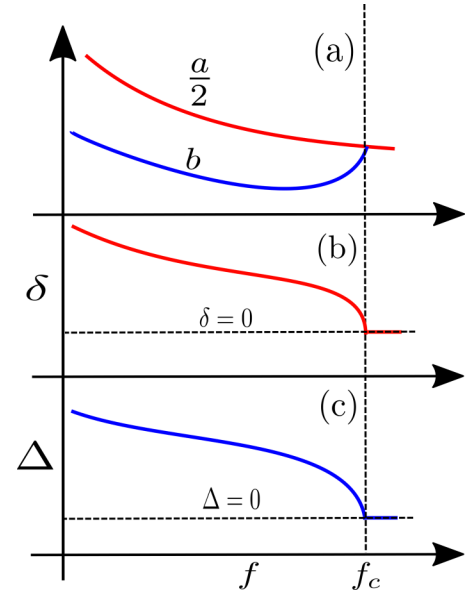


FIG. 14. Schematic representation of the essential results.

data for δ in the correlated [cf. Fig. 15(a)] and noninteracting [cf. Fig. 15(b)] cases, respectively. One sees that a spontaneous Peierls distortion δ_{FE} in that case is about one order of magnitude smaller than that (δ) in the correlated state. The δ_{FE} is practically on the border of our numerical accuracy with the increasing value of f .

Whereas we believe that we have included a remarkable part of electronic correlations in our model, we address the

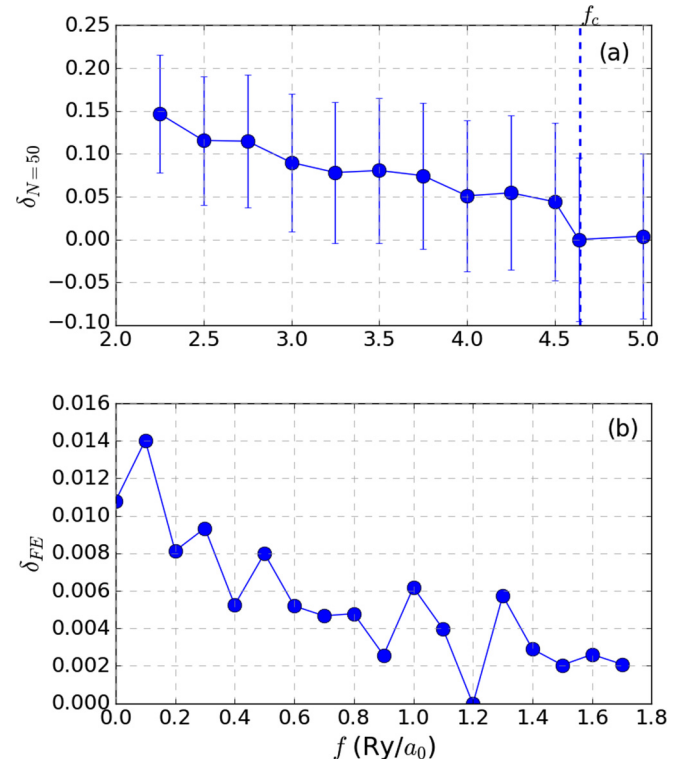


FIG. 15. Distortion evolution parameter obtained by means of the VMC and with $N = 50$ (a) and for the noninteracting electrons (b).

TABLE I. Optimized hopping integrals and atomic energy obtained for $N = 50$.

f (Ry/ a_0)	t_0 (Ry)	t_1 (Ry)	t_2 (Ry)	t_3 (Ry)	t_4 (Ry)	t_5 (Ry)	ϵ (Ry)
2.25	0.0820379	yy - 0.167832	0.67744	- 2.02135	- 2.45895	- 0.27246	- 5.59409
2.5	0.105143	- 0.215954	0.807776	- 2.42219	- 2.79632	- 0.316906	- 5.54753
2.75	0.114176	- 0.231839	0.86109	- 2.57243	- 2.957	- 0.339721	- 5.50698
3	0.125698	- 0.262781	0.928341	- 2.80194	- 3.1156	- 0.355215	- 5.45454
3.25	0.13296	- 0.281589	0.971221	- 2.94012	- 3.21935	- 0.366422	- 5.41488
3.5	0.143846	- 0.300785	1.0376	- 3.12185	- 3.42089	- 0.395242	- 5.33852
3.75	0.147344	- 0.310661	1.05893	- 3.19222	- 3.47167	- 0.400123	- 5.31453
4	0.157736	- 0.344547	1.12335	- 3.4169	- 3.61479	- 0.410421	- 5.23649
4.25	0.167423	- 0.362063	1.18503	- 3.58491	- 3.80312	- 0.436923	- 5.14978
4.5	0.175007	- 0.384558	1.23421	- 3.741	- 3.92157	- 0.448203	- 5.08056
4.635	0.184093	- 0.43643	1.2946	- 4.00422	- 4.00438	- 0.437029	- 4.99011
5	0.188949	- 0.444742	1.32733	- 4.08934	- 4.1061	- 0.451405	- 4.9376

necessity to cover the remaining matrix elements in the Hamiltonian, e.g., correlated hoppings, direct exchange interactions, or even three- of four-center integrals to answer if provided conclusions are undoubtedly valid. Moreover, an inclusion of lattice dynamics and of electron-phonon coupling may provide a valuable outcome both in view of computational (*benchmark*) aspects and physical mechanisms in such phenomenon as conjectured room temperature superconductivity in the metallic hydrogen [47,48].

ACKNOWLEDGMENTS

We thank Adam Rycerz and Michał Zegrodnik for many stimulating and clarifying discussions. The work was financially supported by the Narodowe Centrum Nauki (NCN) through Grant No. DEC-2012/04/A/ST3/00342.

APPENDIX A: MICROSCOPIC PARAMETERS

In Tables I and II we provide all principal microscopic parameters (i.e., $t_{ij}^{\mu\nu}$, ϵ , $K_{ij}^{\mu\nu}$, and U), numbered as in Fig. 1

for the range of forces considered in Fig. 6 for $N = 50$. Note that $f = 4.64(\text{Ry}/a_0)$ and $f = 5(\text{Ry}/a_0)$ refer to a nearly atomic phase. The hopping amplitudes between α and β sites are negative, whereas those between sites from the same sublattice are positive. In the atomic phase [$f \geq 4.64(\text{Ry}/a_0)$], $t_1 \approx t_5$ and $t_3 \approx t_4$, as follows from the symmetry of the atomic system. Similar relations hold for the interaction parameters, i.e., $K_1 \approx K_5$ and $K_3 \approx K_4$. Note that, although U value is the highest, the intersite interactions are up to $\sim 2/3$ of U , which means that we can easily have the situation with $2K \approx U$, which drives the molecular system towards metallization, in addition to the single-particle energy.

APPENDIX B: JASTROW VARIATIONAL PARAMETERS

For the sake of completeness we also present Jastrow variational parameters (cf. Table III) numbered in a similar manner to microscopic parameters. As expected, their amplitudes correspond directly to the magnitude of the interaction parameters.

TABLE II. Electron-electron interaction integrals considered in the optimized state $N = 50$.

f (Ry/ a_0)	K_0 (Ry)	K_1 (Ry)	K_2 (Ry)	K_3 (Ry)	K_4 (Ry)	K_5 (Ry)	U (Ry)
2.25	0.478449	0.627356	0.934136	1.56622	1.63987	0.641265	2.61841
2.5	0.514304	0.675894	1.00048	1.67231	1.72609	0.686352	2.72896
2.75	0.527862	0.693729	1.02576	1.71076	1.76321	0.704012	2.77628
3	0.544872	0.717087	1.05719	1.76318	1.80322	0.725021	2.8324
3.25	0.555068	0.73093	1.07595	1.79338	1.82756	0.737749	2.86468
3.5	0.570171	0.750606	1.10399	1.83494	1.86954	0.757562	2.91719
3.75	0.575004	0.757181	1.11288	1.84936	1.88109	0.763578	2.93283
4	0.589371	0.776929	1.1393	1.89326	1.91453	0.781249	2.97984
4.25	0.60242	0.793848	1.16348	1.92871	1.95109	0.798424	3.02543
4.5	0.612516	0.80744	1.18195	1.95763	1.97542	0.811095	3.05687
4.635	0.624954	0.825457	1.20478	1.99996	1.99997	0.825457	3.09791
5	0.631417	0.833722	1.21668	2.01667	2.01819	0.834038	3.11952

TABLE III. Jastrow wave-function variational parameters for $N = 50$ numbered in the same manner as the microscopic parameters; cf. Table I.

f (Ry/ a_0)	λ_0	λ_1	λ_2	λ_3	λ_4	λ_5	λ_U
2.25	0.0494324	0.0857595	0.151032	0.233874	0.226763	0.0906117	0.543334
2.5	0.0510948	0.0920228	0.161314	0.246269	0.241465	0.0961716	0.567389
2.75	0.0437915	0.0770094	0.131836	0.205208	0.200832	0.0786332	0.479059
3	0.0488745	0.0915902	0.16175	0.244208	0.242687	0.0957701	0.562443
3.25	0.0447105	0.082466	0.144809	0.221195	0.219908	0.0852848	0.513539
3.5	0.0419956	0.0788773	0.141055	0.217371	0.216265	0.0813463	0.504218
3.75	0.0442797	0.0830695	0.143916	0.218546	0.215457	0.0844753	0.502372
4	0.0432848	0.0814832	0.140217	0.21298	0.212156	0.0831675	0.491849
4.25	0.0430579	0.0815563	0.138759	0.210457	0.208788	0.080752	0.484049
4.5	0.0415801	0.0789011	0.135518	0.204778	0.205013	0.0795609	0.472317
4.635	0.0396584	0.0752711	0.128925	0.195331	0.195577	0.0755712	0.450903
5	0.0423223	0.080441	0.13515	0.202073	0.201048	0.0800144	0.461985

- [1] J. Hubbard, Electron correlations in narrow energy bands, *Proc. R. Soc. London* **276**, 238 (1963).
- [2] M. Zegrodnik and J. Spałek, Effect of interlayer processes on the superconducting state within the $t - J - U$ model: Full Gutzwiller wave-function solution and relation to experiment, *Phys. Rev. B* **95**, 024507 (2017).
- [3] J. Spałek, M. Zegrodnik, and J. Kaczmarczyk, Universal properties of high-temperature superconductors from real-space pairing: $t - J - U$ model and its quantitative comparison with experiment, *Phys. Rev. B* **95**, 024506 (2017).
- [4] F. Gebhard, *The Mott Metal-Insulator Transition: Models and Methods* (Springer, Berlin, 1997).
- [5] E. Wigner and H. B. Huntington, On the possibility of a metallic modification of hydrogen, *J. Chem. Phys.* **3**, 764 (1935).
- [6] S. Azadi and W. M. C. Foulkes, Fate of density functional theory in the study of high-pressure solid hydrogen, *Phys. Rev. B* **88**, 014115 (2013).
- [7] J. McMinis, R. C. Clay, D. Lee, and M. A. Morales, Molecular to Atomic Phase Transition in Hydrogen under High Pressure, *Phys. Rev. Lett.* **114**, 105305 (2015).
- [8] N. D. Drummond, B. Monserrat, J. H. Lloyd-Williams, P. López Ríos, Ch. J. Pickard, and R. J. Needs, Quantum Monte Carlo study of the phase diagram of solid molecular hydrogen at extreme pressures, *Nat. Commun.* **6**, 7794 (2015).
- [9] D. Castelvèchi, Physicists doubt bold report of metallic hydrogen, *Nature (London)* **542**, 17 (2017).
- [10] X.-D. Liu, P. Dalladay-Simpson, R. T. Howie, B Li, and E. Gregoryanz, Comment on “observation of the Wigner-Huntington transition to metallic hydrogen”, *Science* **357**, eaan2286 (2017).
- [11] R. P. Dias and I. F. Silvera, Observation of the Wigner-Huntington transition to metallic hydrogen, *Science* **355**, 715 (2017).
- [12] R. T. Howie, Ph. Dalladay-Simpson, and E. Gregoryanz, Evidence for a new phase of dense hydrogen above 325 gigapascals, *Nat. Mater.* **14**, 495 (2015).
- [13] P. Dalladay-Simpson, R. T. Howie, and E. Gregoryanz, Evidence for a new phase of dense hydrogen above 325 gigapascals, *Nature (London)* **529**, 63 (2016).
- [14] M. Borinaga, I. Errea, M. Calandra, F. Mauri, and A. Bergara, Anharmonic effects in atomic hydrogen: Superconductivity and lattice dynamical stability, *Phys. Rev. B* **93**, 174308 (2016).
- [15] S. Azadi, N. D. Drummond, and W. M. C. Foulkes, Nature of the metallization transition in solid hydrogen, *Phys. Rev. B* **95**, 035142 (2017).
- [16] A. P. Kądziaława, A. Biborski, and J. Spałek, Discontinuous transition of molecular-hydrogen chain to the quasiatomic state: Combined exact diagonalization and *ab initio* approach, *Phys. Rev. B* **92**, 161101(R) (2015).
- [17] A. Biborski, A. P. Kądziaława, and J. Spałek, Metallization of solid molecular hydrogen in two dimensions: Mott-Hubbard-type transition, *Phys. Rev. B* **96**, 085101 (2017).
- [18] J. Spałek, R. Podsiadły, W. Wójcik, and A. Rycerz, Optimization of single-particle basis for exactly soluble models of correlated electrons, *Phys. Rev. B* **61**, 15676 (2000).
- [19] J. Spałek, E. M. Görlich, A. Rycerz, and R. Zahorbeński, The combined exact diagonalization-*ab initio* approach and its application to correlated electronic states and Mott-Hubbard localization in nanoscopic systems, *J. Phys.: Condens. Matter* **19**, 255212 (2007).
- [20] A. P. Kądziaława, J. Spałek, J. Kurzyk, and W. Wójcik, Extended Hubbard model with renormalized Wannier wave functions in the correlated state III, *Eur. Phys. J. B* **86**, 252 (2013).
- [21] A. Kądziaława, A. Bielas, M. Acquarone, A. Biborski, M. M. Maška, and J. Spałek, H_2 and $(H_2)_2$ molecules with an *ab initio* optimization of wave functions in correlated state: electron-proton couplings and intermolecular microscopic parameters, *New J. Phys.* **16**, 123022 (2014).
- [22] A. Biborski, A. P. Kądziaława, and J. Spałek, Combined shared and distributed memory *ab-initio* computations of molecular-hydrogen systems in the correlated state: process pool solution and two-level parallelism, *Comput. Phys. Commun.* **197**, 7 (2015).
- [23] A. Rycerz, Ph.D. thesis, Jagiellonian University, 2003, http://www.if.uj.edu.pl/ztns/download/phdTheses/Adam_Rycerz_doktorat.pdf.
- [24] E. Giner, G. L. Bendazzoli, S. Evangelisti, and A. Monari, Full-configuration-interaction study of the metal-insulator transition in model systems: Peierls dimerization in h_n rings and chains, *J. Chem. Phys.* **138**, 074315 (2013).

- [25] F. Becca and S. Sorella, *Quantum Monte Carlo Approaches For Correlated Systems* (Cambridge University Press, Cambridge, UK, 2017).
- [26] R. Rürger, Implementation of the Variational Monte Carlo Method for the Hubbard model, Master's thesis, Goethe University Frankfurt, 2013.
- [27] W. M. C. Foulkes, L. Mitas, R. J. Needs, and G. Rajagopal, Quantum Monte Carlo simulations of solids, *Rev. Mod. Phys.* **73**, 33 (2001).
- [28] L. Stella, C. Attaccalite, S. Sorella, and A. Rubio, Strong electronic correlation in the hydrogen chain: A variational Monte Carlo study, *Phys. Rev. B* **84**, 245117 (2011).
- [29] M. Motta, D. M. Ceperley, G. K.-L. Chan, J. A. Gomez, E. Gull, Sheng Guo, C. A. Jiménez-Hoyos, T. N. Lan, J. Li, F. Ma, A. J. Millis, N. V. Prokof'ev, U. Ray, G. E. Scuseria, S. Sorella, E. M. Stoudenmire, Q. Sun, I. S. Tupitsyn, S. R. White, D. Zgid, and S. Zhang (Simons Collaboration on the Many-Electron Problem), Towards the Solution of the Many-Electron Problem in Real Materials: Equation of State of the Hydrogen Chain with State-of-the-Art Many-Body Methods, *Phys. Rev. X* **7**, 031059 (2017).
- [30] A. Rycerz, Pairwise entanglement and the Mott transition for correlated electrons in nanochain, *New J. Phys.* **19**, 053025 (2017).
- [31] R. E. Peierls, *Quantum Theory of Solids* (Clarendon Press, Oxford, 1955).
- [32] V. Ya. Krivnov and A. A. Ovchinnikov, Peierls instability in weakly nonideal one-dimensional systems, *Zh. Eksp. Teor. Fiz.* **90**, 709 (1986) [*JETP* **63**, 414 (1986)].
- [33] J. E. Hirsch, Effect of Coulomb Interactions on the Peierls Instability, *Phys. Rev. Lett.* **51**, 296 (1983).
- [34] Eric Jeckelmann, Mott-Peierls transition in the extended Peierls-Hubbard model, *Phys. Rev. B* **57**, 11838 (1998).
- [35] P. Umari and N. Marzari, Linear and nonlinear susceptibilities from diffusion quantum Monte Carlo: Application to periodic hydrogen chains, *J. Chem. Phys.* **131**, 094104 (2009).
- [36] H. Watanabe, K. Seki, and S. Yunoki, Charge-density wave induced by combined electron-electron and electron-phonon interactions in $1T - \text{TiSe}_2$: A variational Monte Carlo study, *Phys. Rev. B* **91**, 205135 (2015).
- [37] T. Ohgoe and M. Imada, Variational Monte Carlo method for electron-phonon coupled systems, *Phys. Rev. B* **89**, 195139 (2014).
- [38] P. R. C. Kent, R. J. Needs, and G. Rajagopal, Monte Carlo energy and variance-minimization techniques for optimizing many-body wave functions, *Phys. Rev. B* **59**, 12344 (1999).
- [39] A. Biborski and A. P. Kądziaława, QMT: Quantum Metallization Tools Library, 2014.
- [40] S. Ejima and S. Nishimoto, Phase Diagram of the One-Dimensional Half-Filled Extended Hubbard Model, *Phys. Rev. Lett.* **99**, 216403 (2007).
- [41] G. I. Japaridze, R. M. Noack, D. Baeriswyl, and L. Tincani, Phases and phase transitions in the half-filled $t-t'$ Hubbard chain, *Phys. Rev. B* **76**, 115118 (2007).
- [42] M. Hohenadler, S. Wessel, M. Daghofer, and F. F. Fakher, Interaction-range effects for fermions in one dimension, *Phys. Rev. B* **85**, 195115 (2012).
- [43] L. Wang, H. H. Hung, and M. Troyer, Topological phase transition in the Hofstadter-Hubbard model, *Phys. Rev. B* **90**, 205111 (2014).
- [44] S. Sorella, Y. Otsuka, and S. Yunoki, Absence of a spin liquid phase in the Hubbard model on the honeycomb lattice, *Sci. Rep.* **2**, 992 (2012).
- [45] A. García, T. W. Barbee, M. L. Cohen, and I. F. Silvera, Band gap closure and metallization of molecular solid hydrogen, *EPL (Europhys. Lett.)* **13**, 355 (1990).
- [46] M. Borinaga, J. Ibañez Azpiroz, A. Bergara, and I. Errea, Strong Electron-Phonon and Band Structure Effects in the Optical Properties of High Pressure Metallic Hydrogen, *Phys. Rev. Lett.* **120**, 057402 (2018).
- [47] N. W. Ashcroft, Metallic Hydrogen: A High-Temperature Superconductor? *Phys. Rev. Lett.* **21**, 1748 (1968).
- [48] R. Szcześniak and M. W. Jarosik, Properties of the superconducting state in molecular metallic hydrogen under pressure at 347 GPa, *Physica B (Amsterdam, Neth.)* **406**, 2235 (2011).